Short Papers

A Calibration Method for Odometry of Mobile Robots Based on the Least-Squares Technique: Theory and Experimental Validation

Gianluca Antonelli, Stefano Chiaverini, and Giuseppe Fusco

***Abstract*—For a mobile robot, odometry calibration consists of the identification of a set of kinematic parameters that allow reconstructing the vehicle's absolute position and orientation starting from the wheels' encoder measurements. This paper develops a systematic method for odometry calibration of differential-drive mobile robots. As a first step, the kinematic equations are written so as to underline linearity in a suitable set of unknown parameters; thus, the least-squares method can be applied to estimate them. A major advantage of the adopted formulation is that it provides a quantitative measure of the optimality of a test motion; this can be exploited to drive guidelines on the choice of the test trajectories and to evaluate accuracy of a solution. The proposed technique has been experimentally validated on two different mobile robots and, in one case, compared with other existing approaches; the obtained results confirm the effectiveness of the proposed calibration method.**

***Index Terms*—Calibration, identification, mobile robot kinematics, mobile robots, parameter estimation.**

I. Introduction

For wheeled mobile robots, the use of encoders' measurements at the wheels to reconstruct the absolute configuration (i.e., position and orientation) of the vehicle's body is called odometry. Starting from a known configuration, the current position and orientation of the robot is obtained by time integration of the vehicle's displacement corresponding to the commanded wheels' displacement. As such, odometry is affected by three main sources of error:

- systematic errors, i.e., build-up of the modeling error due to the parameter uncertainties in the kinematics equation used to convert the wheel's displacements into the vehicle's displacements;
- nonsystematic errors, such as those due to wheel slippage or uneven ground;
- numerical drift, inherently related to discrete-time integration of the relevant displacements.

Recently, it has been recognized that the overall error in reconstructing the vehicle's absolute configuration drifts by showing a square dependence with the distance traveled [15], [16]. Nevertheless, since accuracy of a discrete-time integration can be improved by suitably shortening the sampling period or changing the integration rule, the amplitude of the error is most influenced by the uncertainty in the kinematic parameters.

Odometry calibration is the process aimed at identifying the kinematic parameters used to reconstruct the robot's absolute configuration from measurements at the wheels. A mobile robot with well-calibrated odometry can safely travel a long path before requiring a reset of the drifting odometric error; this can be achieved through direct measurement of the absolute configuration as given by, e.g., a global positioning system (GPS).

From a general point of view, the existing methods aimed at correcting the vehicle's odometry are either geometric-based or rely on multisensory data fusion. Another possible distinction regards how the calibration technique interacts with motion control of the robot. In this respect, it is possible to either devise methods that calibrate the odometry offline (e.g., through periodic execution of suitable test trajectories) or pursue calibration techniques that update the odometry online (e.g., by taking advantage of etheroceptive sensory data).

In the frame of geometric-based approaches, one of the first papers that concentrate on odometric errors is [24], where knowledge of the path under execution is used to improve posture estimation between odometric updates. Another geometric method is presented in [8], which performs identification of the odometric parameters based on absolute position measurements after the execution of a set of suitably defined trajectories; the possibility of obtaining poor results because of a wrong choice of the test trajectory is also discussed on a heuristic basis. Recently, the latter method has been experimentally compared in [11] with an algorithm based on the boundedness property of the error for generalized Voronoi graph-based paths.

Among the approaches resorting to multisensory systems, [23] develops an iterative algorithm to identify a set of unknown parameters, where the odometric parameters are a subset of all the estimated ones; in the reported experimental results, the wheel radii are not identified. In [17], a sensor-fusion technique is proposed, where in order to improve accuracy of the robot configuration estimate, odometry is used together with direct measurement of absolute angular velocity provided by an optical-fiber gyroscope; however, a drift on the estimate still persists. Multisensory measurement is also exploited in [22], where a laser sensory system is used to correct online the odometry through a maximum-likelihood-based identification technique. The paper [12] uses a gyroscope, together with the encoders, and a GPS unit in a Kalman-filter approach, in order to estimate the outdoor robot's configuration; another multisensory system, applied to a car-like vehicle, is presented in [6]. An internal (i.e., not based on direct absolute measurements) error-position-correction technique is presented in [7] for a two-truck vehicle; to this purpose, however, the system is equipped with a redundant odometric system.

Some recent papers attempt an analytic characterization of the odometric errors. Along these lines, an odometric error model aimed at reducing nonsystematic errors is developed in [9]. References [19] and [20] present a method to identify two systematic and two nonsystematic errors. In [15] and [16], the error propagation in vehicle odometry is analytically discussed, and two main results are given: quadratic dependency of the estimation error with respect to the distance traveled, and existence of path-independent systematic errors.

In this paper, following the research reported in [4] and [5], a systematic method for odometry calibration of differential-drive mobile robots is developed. As a first step, the kinematic equations are written so as to underline linearity in a suitable set of unknown parameters that relate the motion inputs to the measurements. This approach naturally leads to a linear identification problem that allows application of the least-squares (LS) method. Different from heuristically developed algorithms, a major advantage inherited by the adopted formulation from

Manuscript received September 9, 2004; revised January 11, 2005 and February 25, 2005. This paper was recommended for publication by Associate Editor W. Chung and Editor S. Hutchinson upon evaluation of the reviewers' comments.

The authors are with the Dipartimento di Automazione, Elettromagnetismo, Ingegneria dell'Informazione e Matematica Industriale (DAEIMI), Università degli Studi di Cassino, 03043 Cassino (FR), Italy (e-mail: antonelli@unicas.it; chiaverini@unicas.it; fusco@unicas.it).

Digital Object Identifier 10.1109/TRO.2005.851382

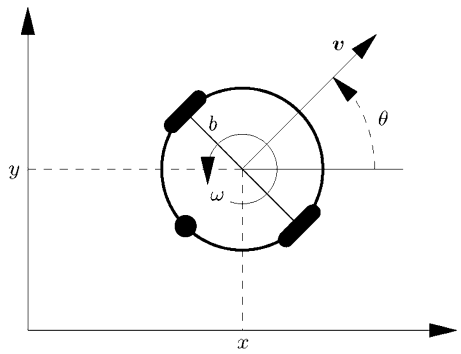

Fig. 1. Top-view sketch of a differential-drive mobile robot with relevant variables.

the LS technique is that it provides a measure of the numerical conditioning of the data; this can be exploited to drive guidelines on the choice of the test trajectories and to evaluate accuracy of a solution. An experimental study on two different differential-drive mobile robots finally confirms the effectiveness of the proposed odometry-calibration method, also in comparison with other existing approaches.

II. Modeling

Let us consider a differential-drive mobile robot as sketched in Fig. 1. The motion of the left and right wheels is characterized by the sole (scalar) axis angular velocities ω_L and ω_R, respectively; the rear castor wheel is passive.

Let us consider a ground-fixed inertial reference frame Σ_i. By defining as *wheelbase* the segment of length b connecting the two lateral wheels along their common axis, it is convenient to choose a vehicle-fixed frame Σ_v such as the following: its origin is at the middle of the wheelbase, its x axis points toward the front of the robot body, and its y axis points toward the left wheel, completing a right-hand frame. With this choice, the absolute velocity of the robot body can be described by the two-dimensional (2-D) vector $\boldsymbol{v}$, expressing the translational velocity of the origin of Σ_v with respect to Σ_i, and by the scalar ω expressing the angular velocity of Σ_v as seen from Σ_i.

A major advantage of the above choice is that, under the assumption that the wheels do not slide on the ground, the translational velocity $\boldsymbol{v}$ is always orthogonal to the wheelbase. Therefore, in the vehicle-fixed frame, the vector $\boldsymbol{v}$ is completely characterized by its sole x-component, denoted as v.

It can be recognized (see Fig. 1) that the body-fixed components v and ω of the robot velocity are related to the angular velocity of the wheels by

$$\begin{bmatrix} v \\ \omega \end{bmatrix} = \boldsymbol{C} \begin{bmatrix} \omega_R \\ \omega_L \end{bmatrix} \tag{1}$$

where the matrix $\boldsymbol{C} \in \mathbb{R}^{2\times 2}$ is defined as

$$\boldsymbol{C} = \begin{bmatrix} \frac{r_R}{2} & \frac{r_L}{2} \\ \frac{r_R}{b} & -\frac{r_L}{b} \end{bmatrix} \tag{2}$$

in which r_R and r_L are the radii of the right and left wheel, respectively.

By further denoting as x and y the coordinates of the origin of Σ_v expressed in the frame Σ_i, and as θ the heading angle between the x axis of Σ_v and Σ_i, the robot kinematic equations are written in the unicycle-like form

$$\begin{cases} \dot{x} = v\cos(\theta) \\ \dot{y} = v\sin(\theta) \\ \dot{\theta} = \omega. \end{cases} \tag{3}$$

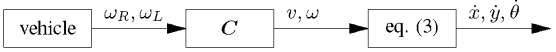

Fig. 2. Kinematic transformations from wheel velocities, to body-fixed components of robot velocities and to ground-fixed components of robot velocities.

The relationships among the above kinematic transformations are summarized in Fig. 2.

The odometry of a vehicle is usually implemented by discrete-time integration of (3), such as

$$\begin{cases} x_{k+1} = x_k + T v_k \cos(\theta_k + T\omega_k/2) \\ y_{k+1} = y_k + T v_k \sin(\theta_k + T\omega_k/2) \\ \theta_{k+1} = \theta_k + T\omega_k \end{cases} \tag{4}$$

where the subscript k denotes the kth time sample and T is the sampling period. Notice that low sampling frequency and high vehicle velocities can be a significant source of odometric error.

III. Proposed Calibration Technique

To estimate the current vehicle configuration, the odometry performs a numerical integration of the absolute vehicle velocity $\dot{x}$, $\dot{y}$, $\dot{\theta}$ given by (3), e.g., by computing (4). To this purpose, one must first estimate v_k and ω_k through (1), starting from measurement of ω_R and ω_L at the kth time sample. On the other hand, the inverse mapping of (1) is used by the motion-control system to compute the reference angular velocity of the wheels corresponding to an assigned desired velocity of the vehicle.

The computation of the matrix $\boldsymbol{C}$, appearing in (1), is performed with the available estimate $\hat{b}$, $\hat{r}_R$, $\hat{r}_L$ of the odometric parameters. This naturally poses an identification problem aimed at minimizing the reconstruction error related to the mismatching between actual and estimated parameters in $\boldsymbol{C}$.

Most algorithms aimed at identifying the vehicle odometry pursue the direct estimate of the single odometric parameters b, r_R, and r_L. However, according to (2), these are combined in a nonlinear fashion in the expression of the matrix $\boldsymbol{C}$, which poses a nonlinear identification problem. A possible way to simplify the solution of this problem is to execute specific motion trajectories designed to excite the single parameters' contribution. Another approach that works directly on the odometric parameters is the algorithm proposed in [8], where knowledge of the average wheel diameter is assumed; of course, accuracy of this data directly influences the estimate of the other odometric parameters.

The idea under the proposed technique is to identify the four elements $c_{i,j}$ of the matrix $\boldsymbol{C}$, instead of the three odometric parameters. In fact, while in view of the implementation of a calibrated odometry the result is numerically the same as that that would be achieved by estimating the single odometry parameters, our approach leads to a linear identification problem. On the other hand, while from a physical point of view, the unknowns are only three—namely, the wheelbase and the two wheels' radii—, by estimating the four elements of the matrix $\boldsymbol{C}$ as if they were independent, our identification process ignores their mutual relationship. Redundancy in the unknowns, however, is not new to calibration methods; for example, the algorithm in [8] ends up with two sets of different equations that give the same three unknowns.

Let us rewrite the third equation in (4) so as to exploit linearity in the four parameters $c_{i,j}$. Across the first time increment, it is

$$\theta_1 = \theta_0 + T\, c_{2,1}\, \omega_{R,0} + T\, c_{2,2}\, \omega_{L,0} \tag{5}$$

that, iterated up to the final Nth time sample of a generic trajectory, yields

$$\theta_N - \theta_0 = T\, c_{2,1} \sum_{i=0}^{N-1} \omega_{R,i} + T\, c_{2,2} \sum_{i=0}^{N-1} \omega_{L,i}. \tag{6}$$

By defining the (1×2) regressor

$$\boldsymbol{\Phi}_\theta = T \left[\sum_{i=0}^{N-1} \omega_{R,i} \quad \sum_{i=0}^{N-1} \omega_{L,i} \right] \tag{7}$$

(6) can be written in compact form as

$$\theta_N - \theta_0 = \boldsymbol{\Phi}_\theta \begin{bmatrix} c_{2,1} \\ c_{2,2} \end{bmatrix}. \tag{8}$$

Notice that the initial and final vehicle orientations to be used in (8) need to be obtained by absolute measurements using, e.g., a camera or a geometric triangulation with the vehicle still at the start and the end of the considered motion trajectory.

As usual in batch LS estimation, sufficient data must be collected in a number of different experiments. By assuming to execute P suitable trajectories and collecting the results in stacked form, one has

$$\begin{bmatrix} \theta_{N,1} - \theta_{0,1} \\ \vdots \\ \theta_{N,P} - \theta_{0,P} \end{bmatrix} = \begin{bmatrix} \boldsymbol{\Phi}_{\theta,1} \\ \vdots \\ \boldsymbol{\Phi}_{\theta,P} \end{bmatrix} \begin{bmatrix} c_{2,1} \\ c_{2,2} \end{bmatrix} = \bar{\boldsymbol{\Phi}}_\theta \begin{bmatrix} c_{2,1} \\ c_{2,2} \end{bmatrix} \tag{9}$$

which leads to defining the $(P \times 2)$ regressor $\bar{\boldsymbol{\Phi}}_\theta$. The reconstruction error over the angle data collected in the P trajectories is then minimized in a LS sense by estimating the unknown parameters $c_{2,1}$ and $c_{2,2}$ as

$$\begin{bmatrix} \hat{c}_{2,1} \\ \hat{c}_{2,2} \end{bmatrix} = \left(\bar{\boldsymbol{\Phi}}_\theta^{\mathrm{T}} \bar{\boldsymbol{\Phi}}_\theta \right)^{-1} \bar{\boldsymbol{\Phi}}_\theta^{\mathrm{T}} \begin{bmatrix} \theta_{N,1} - \theta_{0,1} \\ \vdots \\ \theta_{N,P} - \theta_{0,P} \end{bmatrix}. \tag{10}$$

A similar approach for the position coordinates leads, over a single trajectory, to the following equation:

$$\begin{bmatrix} x_N - x_0 \\ y_N - y_0 \end{bmatrix} = \boldsymbol{\Phi}_{xy} \begin{bmatrix} c_{1,1} \\ c_{1,2} \end{bmatrix} \tag{11}$$

where

$$\begin{bmatrix} x_N - x_0 \\ y_N - y_0 \end{bmatrix} \tag{12}$$

is the vector of measurements and

$$\boldsymbol{\Phi}_{xy} = T \begin{bmatrix} \sum_{i=0}^{N-1} \omega_{R,i} \cos(\theta_i + T\omega_i/2) & \sum_{i=0}^{N-1} \omega_{L,i} \cos(\theta_i + T\omega_i/2) \\ \sum_{i=0}^{N-1} \omega_{R,i} \sin(\theta_i + T\omega_i/2) & \sum_{i=0}^{N-1} \omega_{L,i} \sin(\theta_i + T\omega_i/2) \end{bmatrix} \tag{13}$$

is the (2×2) regressor matrix. To compute (13), an unbaised estimate of θ_i and ω_i is needed. One such estimate can be obtained from the third equation in (4) and the second row in (1); in this way, however, a biased error in the estimation of the first two elements of $\boldsymbol{C}$ is propagated to the estimation of the remaining elements. On the other hand, the vehicle position at the initial and final time sample can be determined with several methods [8].

By executing P trajectories and stacking the obtained regressors (13) in a single $(2P \times 2)$ matrix $\bar{\boldsymbol{\Phi}}_{xy}$, the LS estimate of the unknown parameters $c_{1,1}$ and $c_{1,2}$ is

$$\begin{bmatrix} \hat{c}_{1,1} \\ \hat{c}_{1,2} \end{bmatrix} = \left(\bar{\boldsymbol{\Phi}}_{xy}^{\mathrm{T}} \bar{\boldsymbol{\Phi}}_{xy} \right)^{-1} \bar{\boldsymbol{\Phi}}_{xy}^{\mathrm{T}} \begin{bmatrix} x_{N,1} - x_{0,1} \\ y_{N,1} - y_{0,1} \\ \vdots \\ x_{N,P} - x_{0,P} \\ y_{N,P} - y_{0,P} \end{bmatrix}. \tag{14}$$

The C matrix estimated in this way may not satisfy the physical constraint of $c_{1,1}/c_{1,2} = -c_{2,1}/c_{2,2}$. It is worth noticing that it might be possible to include this constraint in the estimation procedure after $\hat{c}_{1,1}$ and $\hat{c}_{1,2}$ have been obtained, leading to an equation corresponding to (14) with only one unknown. Being a model with a smaller number of parameters, however, a larger reconstruction error might be experienced.

IV. Guidelines for Setting Up the Calibration Procedure

As is well known in identification of industrial robot dynamic parameters, the choice of the trajectories used to collect the measurement data is a crucial aspect. In fact, a wrong choice of the test trajectories results in ill-conditioned data that severely affects numerical accuracy of the LS solution.

Given the following linear relationship:

$$\boldsymbol{y} = \boldsymbol{W}\boldsymbol{c} + \boldsymbol{\rho} \tag{15}$$

where $\boldsymbol{y} \in \mathbb{R}^n$ is a measurement data vector, $\boldsymbol{W} \in \mathbb{R}^{n \times p}$ (with $n > p$) is a deterministic regressor, $\boldsymbol{c} \in \mathbb{R}^p$ is the vector of unknown parameters, and $\boldsymbol{\rho} \in \mathbb{R}^n$ is the measurement noise, the following constraint holds [21]:

$$\frac{\|\tilde{\boldsymbol{c}}\|}{\|\boldsymbol{c}\|} \leq \mathrm{cond}(\boldsymbol{W}) \frac{\|\boldsymbol{\rho}\|}{\|\boldsymbol{y}\|} \tag{16}$$

where $\tilde{\boldsymbol{c}} = \boldsymbol{c} - \hat{\boldsymbol{c}}$ is the estimation error. Moreover, given a scalar noise variance σ_ρ^2, the covariance matrix of the estimation error $E[\tilde{\boldsymbol{c}}\tilde{\boldsymbol{c}}^{\mathrm{T}}]$ is given by

$$E[\tilde{\boldsymbol{c}}\tilde{\boldsymbol{c}}^{\mathrm{T}}] = \sigma_\rho^2 \left[\boldsymbol{W}^{\mathrm{T}} \ \boldsymbol{W} \right]^{-1}. \tag{17}$$

The 2-norm of a matrix is its largest singular value [13], hence, the norm of the covariance matrix of the estimation error can be computed by knowing the smallest singular value of $\boldsymbol{W}$ as

$$\|E[\tilde{\boldsymbol{c}}\tilde{\boldsymbol{c}}^{\mathrm{T}}]\| = \left(\frac{\sigma_\rho}{\lambda_{\min}(\boldsymbol{W})} \right)^2. \tag{18}$$

Equations (16)–(18) clearly show the importance of using a proper set of data for the identification procedure. Roughly speaking, besides a low measurement noise, a large norm of the data vector $\boldsymbol{y}$ and a well-balanced (i.e., low condition number with high minimum singular value) regressor $\boldsymbol{W}$ are required to ensure good numerical conditioning of the LS problem.

The above relations can be exploited to drive some useful guidelines for setting up the calibration procedure, usually involving several test trajectories, for our method. In particular, with reference to the orientation part of the problem, it is

$$\boldsymbol{y} = \begin{bmatrix} \theta_{N,1} - \theta_{0,1} \\ \vdots \\ \theta_{N,P} - \theta_{0,P} \end{bmatrix} \quad \boldsymbol{W} = \bar{\boldsymbol{\Phi}}_\theta \quad \boldsymbol{c} = \begin{bmatrix} c_{2,1} \\ c_{2,2} \end{bmatrix}$$

while for the translational part

$$\boldsymbol{y} = \begin{bmatrix} x_{N,1} - x_{0,1} \\ y_{N,1} - y_{0,1} \\ \vdots \\ x_{N,P} - x_{0,P} \\ y_{N,P} - y_{0,P} \end{bmatrix} \quad \boldsymbol{W} = \bar{\boldsymbol{\Phi}}_{xy} \quad \boldsymbol{c} = \begin{bmatrix} c_{1,1} \\ c_{1,2} \end{bmatrix}.$$

Since, in our case, the measurement data vector collects the total angular and translational displacements over the single trajectories, a high-norm requirement for it makes preferable the use of trajectories with open path and constant-sign curvature. On the other hand, either closed paths or paths with identically null or mutually compensating curvatures (e.g., rectilinear or S-shaped, respectively) are not suited to our calibration technique. In fact, since a good noncalibrated odometry allows accurate path tracking, on these paths, it would obtain a small norm of $\boldsymbol{y}$, whereas a poorly calibrated odometry might loose the path and yield a large norm of $\boldsymbol{y}$. Therefore, being $\boldsymbol{y}$ measured by external absolute sensors, these paths would lead to a paradox: the better the noncalibrated odometry, the worse the numerical balance of the LS solution. Closed paths with mutually compensating curvatures (e.g., 8-shaped) are the worst choice, since they yield low norm for both the angular and the translational data.

To raise the norm of the measurement data vector, a *long* path involving a *large* rotation of the vehicle body would then seem to qualify as a good choice for the test trajectory. However, it must be noticed that in the case of mobile robots, the probability of the occurrence of nonsystematic errors grows with the distance traveled; this results in a practical upper bound to the length of paths for odometry calibration. It must be remarked that (16) is a dimensionless relationship; therefore, to qualify a length or a rotation as large, one must compare with the amount of measurement noise, depending on the available sensors, experienced through the value of the regressor elements.

As for the need of ensuring a well-balanced regressor $\boldsymbol{W}$, it is difficult to predict the quality of a test trajectory in the general case, because for a generic path, the regressor does not have a simple closed-form expression; however, this analysis may become affordable for paths of simple geometry. For example, in the case of a square path, it can be verified that the regressor $\bar{\boldsymbol{\Phi}}_{xy}$ is badly scaled. On the other hand, it can be recognized that paths perceived as closed by the odometry lead to a badly scaled regressor $\bar{\boldsymbol{\Phi}}_{\theta}$. These are additional reasons to avoid closed paths with our calibration technique.

Another general drawback related to the use of closed paths for calibration purposes is that the effects of path-independent systematic errors, such as those described in [16], vanish on them. Moreover, [8] observed that paths as the 8-shaped path [10] or the unidirectional square path [17] may not be appropriate; in fact, bidirectional paths reduce the effects of systematic errors. In particular, the bidirectional square path results in an efficient calibration trajectory for our method only if the noncalibrated odometry is affected by a large error at least in one of the rotation directions.

Finally, as pointed out in [21], if bad scaling of the problem comes from a much different magnitude of the parameters to be estimated (i.e., small and large values together), a better balance of the numerical problem can be achieved by proper weighting. In detail, by considering an *a priori* knowledge of the parameters, e.g., their nominal value $\boldsymbol{c}_n$, (15) can be rewritten as

$$\boldsymbol{y} = \boldsymbol{W}\,\mathrm{diag}(\boldsymbol{c}_n)\mathrm{diag}(\boldsymbol{c}_n)^{-1}\boldsymbol{c} + \boldsymbol{\rho}$$

that letting

$$\bar{\boldsymbol{W}} = \boldsymbol{W}\,\mathrm{diag}(\boldsymbol{c}_n) \quad \bar{\boldsymbol{c}} = \mathrm{diag}(\boldsymbol{c}_n)^{-1}c$$

becomes

$$\boldsymbol{y} = \bar{\boldsymbol{W}}\bar{\boldsymbol{c}} + \boldsymbol{\rho}. \tag{19}$$

It can be recognized that the elements of the vector $\bar{\boldsymbol{c}}$ are close to unity, resulting in a good numerical scaling of the problem.

V. Experimental Case Studies

The proposed calibration technique has been validated in experiments on two commercial differential-drive mobile robots; namely, the Khepera II manufactured by K-Team and the Magellan PRO manufactured by Real World Interface. While the two robots are both of differential-drive type, they are of much different dimensions and have different hardware-software architectures; this requires consideration of different implementation issues, as detailed in the following. This section also describes the vision-based absolute measurement system used to obtain the data vectors, and the criteria adopted to properly evaluate the results obtained by using different calibration techniques in comparison.

A. Criteria Adopted to Report the Results

In the wide literature on calibration techniques, although there is not a uniform way of evaluating goodness of the obtained results, most papers report some kind of odometric error as a figure to measure the achieved performance. While this suffices to evaluate a single technique over a single motion for a given mobile robot, it reveals to be inadequate for a more general performance assessment aimed, e.g., at comparing different techniques over different trajectories possibly executed by different mobile robots. Of course, while the latter goal might reasonably appear too ambitious, there are some points to be considered if proper comparison of different calibration methods is pursued as in the case study of this paper.

One first thing to be underlined is that, while the classical identification theory suggests using a different—but *similar*—set of data with respect to those used for the identification itself [18], the validation obtained using the same data of the calibration can give qualitative information about the relevant presence of unmodeled nonlinear effects (e.g., quantization, friction).

One further point to be considered in comparing two different calibration techniques on the same given trajectory is that they will probably run in different conditions. Dually, since some errors tend to mutually compensate for some specific trajectories, the same calibration technique might give different results over different paths.

To witness quality of the proposed calibration technique, a number of papers report the improvement achieved by their method with respect to the pre-existing odometry. Of course, this approach does not give an absolute performance index and, moreover, may finally be misleading: starting from a poor pre-existing odometry, even a plain calibration method can result in a significant improvement.

A possible global performance index for a given odometry calibration is the maximum error obtained over a set of trajectories; however, due to the possible occurrence of large nonsystematic errors (even a single one), a good calibration technique may show bad performance. For this reason, it is advisable to consider, besides the maximum value of the error, some other information about its statistic distribution, e.g., the mean value and the standard deviation.

Finally, it must be pointed out that the value of the odometric error grows with the motion length. Although this dependence is nonlinear, it is usual practice to normalize the absolute error with respect to the distance traveled (or the total angle rotated). Nevertheless, notice that nonsystematic errors occur with larger probability over long paths than over short ones.

According to the above, in reporting the experimental results related to the case study developed in this paper:

- the odometric error is considered both for a set of motion data used for the calibration and for a set of motion data not used for the calibration;
- each validation trajectory is considered for all the calibrations under comparison, and each calibration is used for all the validation trajectories;
- as an aggregate value for the errors obtained for each set of trajectories, we consider the normalized error defined as

$$\mathrm{err}_{\%} = 100\frac{\mathrm{err}}{\Delta}$$

where "err" is the norm of the average position error or the absolute value of the average orientation error, and Δ is the overall distance or angle traveled. Of course, $\mathrm{err}_{\%}$ should be zero for a perfect calibration in the absence of nonsystematic errors. In addition, the maximum of the norm (absolute value) of the position error (orientation error) is also reported, together with the errors' standard deviation on all the data of each set considered. Concerning the position error, please notice that the *mean* and the *std* values are computed on the two components with their sign, then a norm is computed in order to have a representative scalar value instead of a vector of two elements. The maximum, instead, is computed by considering the norm of the absolute error for each trajectory.

B. Description of the Vision-Based Measurement System

Experiments of odometry calibration require measurement of the absolute position and orientation of the mobile robot at suitable locations along the motion trajectories. For instance, as detailed in Section III, our calibration technique requires measurement of the starting and final robot configuration for each motion execution.

To allow the needed absolute measurements, we have developed a vision-based system using a charge-coupled device (CCD) monochrome camera, the Matrox Meteor-II frame grabber, and the C++ image-processing functions of the Matrox Imaging Library (MIL) [3]. The acquired images are 640×480 black-and-white bitmaps with 256 grey levels.

The calibration of the camera is performed with a custom algorithm that has been cross-checked with the standard algorithm provided by the MIL library, leading to an average pixel error of few millimeters over a $\approx 160 \times 120$ cm scene. The camera model corresponds to a standard pinhole projection [14]. The camera is placed overhead the scene; however, to exactly extract the absolute vehicle position at the ground level, the homogeneous transformation from the camera to the inertial reference frame is also identified. Let us define as $\boldsymbol{f}_c = [f_{c,1}\ f_{c,2}]^{\mathrm{T}} \in \mathbb{R}^2$ the effective focal lengths, and as $\boldsymbol{c}_c \in \mathbb{R}^2$ the principal point, both expressed in pixels. The vector $\boldsymbol{p}^c = [x^c\ y^c\ z^c]^{\mathrm{T}} \in \mathbb{R}^3$ is a point in the camera reference frame, expressed in meters. The pinhole projection is defined as

$$\boldsymbol{p}^p = \begin{bmatrix} f_{c,1} & 0 \\ 0 & f_{c,2} \end{bmatrix} * \begin{bmatrix} x^c/z^c \\ y^c/z^c \end{bmatrix} + \boldsymbol{c}_c. \tag{20}$$

The given point can be expressed in a different reference frame, e.g., an inertial frame, $\boldsymbol{p}^v \in \mathbb{R}^3$ by the known relation

$$\boldsymbol{p}^c = \boldsymbol{R}_v^c \boldsymbol{p}^v + \boldsymbol{t}_c \tag{21}$$

where $\boldsymbol{R}_v^c \in \mathbb{R}^{3\times 3}$ is the rotation from the inertial to the camera-fixed frame, and $\boldsymbol{t}_c \in \mathbb{R}^3$ is the vector connecting the camera-fixed frame to the inertial frame expressed in the camera frame. The camera calibration procedure identifies the 10 unknowns represented by $\boldsymbol{f}_c$, $\boldsymbol{c}_c$, $\boldsymbol{t}_c$, and three independent rotation parameters that allow computing the matrix $\boldsymbol{R}_v^c$.

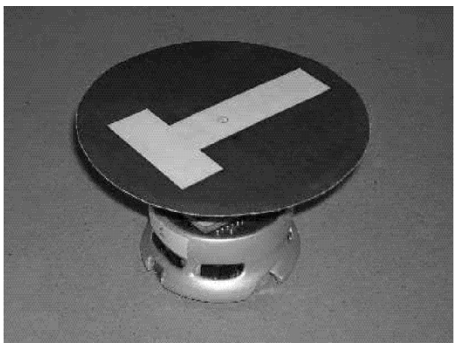

Fig. 3. Picture of the Khepera II together with the T-shaped model used to estimate its position and orientation.

Fig. 4. Khepera II mobile robot.

Once the camera has been calibrated, the vehicle configuration with respect to an inertial frame is obtained by resorting to model finder techniques. A picture of the Khepera II together with the T-shaped model used to locate the robot is reported in Fig. 3; notice that, in view of the small size of the Khepera II, to increase accuracy of the measurement, we have chosen to use a geometric model slightly exceeding the robot dimensions. As for the Magellan PRO, an L-shaped model has been used to locate the robot that is shown in the forthcoming Fig. 10. Remarkably, since estimation of the robot configuration is done with the vehicle stopped, in the absence of real-time computational constraints, accurate iterative techniques of geometric model finder can be applied. The bottleneck is then set by the camera resolution.

C. Experiments With the Khepera II

A first set of experiments has been run with the robot Khepera II, shown in Fig. 4, manufactured by K-Team [2].

The sampling period used is 50 ms; this choice has been strongly influenced by the use of the serial link to a remote host PC running the motion-control algorithm and caring storage of the data.

To avoid slippage of the wheels that causes the occurrence of nonsystematic errors, all the trajectories have blended polynomial time laws so as to guarantee continuity of the desired position, velocity, and acceleration variables all over the motion. Notice that unless differently stated, in this subsection, the lengths are reported in centimeters and the angles in radians.

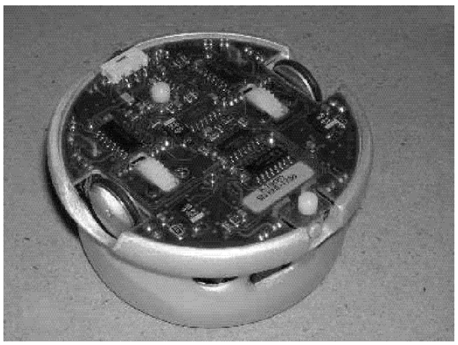

Fig. 5. Picture of the bottom part of the Khepera II; it is worth noticing the presence of a rubber ring around the aluminum body of the wheels.

The calibration has been performed by resorting to three different methods:

A) direct measurement of the odometric parameters;
B) the UMBmark technique described in [8];
C) the technique proposed in this paper.

While application of Method A) obviously does not require execution of a test motion, in our case, it requires accurate measurement of the wheels' radius and the wheelbase. In view of the small size of the robot and due to the presence of a rubber ring around the aluminum body of the wheels (see Fig. 5), our best measurement does not allow appreciating differences between the radii r_R and r_L, that are both estimated to be about 8 mm. The wheelbase is 53 mm long. Therefore, the $\boldsymbol{C}$ matrix obtained by Method A) is

$$\boldsymbol{C}_A = \begin{bmatrix} 0.40 & 0.40 \\ 0.15 & -0.15 \end{bmatrix}.$$

Application of Method B) requires measurement of the average diameter of the wheels and the execution of square-path test motions. Since a measurement error on the average wheel diameter propagates to the overall calibration results, the average diameter of the wheels has been estimated in two ways. First by using direct measurements and then by reconstructing its value from the matrix C identified with the method proposed in this paper; the value that gave better results has finally been adopted. It is worth noticing that in [8], with a different mobile robot, an indirect measurement strategy could be applied resulting in a better estimation. According to the guidelines in [8], the test motions are a set of 10 trajectories (briefly **set1** in the following) that describe a square path five times clockwise (CW) and five times counterclockwise (CCW) to avoid compensation of the errors; the square side has been scaled to 40 cm to better adapt the path length to the size of the Khepera II. Each trajectory consists in a chain of four elementary motion pairs made by a pure 40-cm translation and a pure $\pi/2$-rad rotation executed each with a fifth-order polynomial time law. The $\boldsymbol{C}$ matrix obtained by Method B) is

$$\boldsymbol{C}_B = \begin{bmatrix} 0.3999 & 0.4001 \\ 0.1495 & -0.1495 \end{bmatrix}.$$

Finally, application of Method C) requires the execution of suitable test motions. Following the guidelines discussed in Section IV, the test trajectories to calibrate the odometry should achieve large norm of the data vector while keeping a small condition number of the regressors; this is obtained in our case with nine open paths, each consisting of circular motion segments of different diameters. In detail, each path consists of a odd number of semicircles that result in an approximately equal distance traveled over the different paths. The time law is a blend of a constant-speed cruise phase with fifth-order polynomials in the acceleration and deceleration phases. To avoid compensation of the errors, each path is described both in the CW and in the CCW direction, leading to a set of 18 trajectories (briefly **set2** in the following). The data collected by the test trajectories result in the regressors' condition numbers

$$\begin{aligned} \mathrm{cond}(\bar{\boldsymbol{\Phi}}_\theta) &= 3.2 \\ \mathrm{cond}(\bar{\boldsymbol{\Phi}}_{xy}) &= 4.9 \end{aligned}$$

in the data vectors' norm

$$\left\| \begin{bmatrix} \theta_{N,1} - \theta_{0,1} \\ \vdots \\ \theta_{N,18} - \theta_{0,18} \end{bmatrix} \right\| = 166$$

$$\left\| \begin{bmatrix} x_{N,1} - x_{0,1} \\ y_{N,1} - y_{0,1} \\ \vdots \\ x_{N,18} - x_{0,18} \\ y_{N,18} - y_{0,18} \end{bmatrix} \right\| = 105$$

and in the smallest singular values

$$\begin{aligned} \lambda_{\min}(\bar{\boldsymbol{\Phi}}_\theta) &= 777 \\ \lambda_{\min}(\bar{\boldsymbol{\Phi}}_{xy}) &= 39. \end{aligned}$$

These values guarantee that the numerical problem is well defined [cfr. (16) and (18)]. The $\boldsymbol{C}$ matrix obtained by Method C) is

$$\boldsymbol{C}_C = \begin{bmatrix} 0.4009 & 0.3772 \\ 0.1508 & -0.1511 \end{bmatrix}.$$

After the three calibrations, other trajectories have been run to validate the three obtained odometries and to evaluate the experimental results. Overall, the following sets of trajectories have been considered:

set1 10 trajectories, five CW and five CCW, over a square path of 40-cm side;
set2 18 trajectories, nine CW and nine CCW, over open circular paths of different radii;
set3 10 trajectories, five CW and five CCW, over other open paths obtained by performing only two side and two rotations of the square path of **set1**.

Notice that the **set1** and **set2** trajectories include also those used for the calibration Methods B) and C), respectively, while the **set3** trajectories include pure validation data. Table I reports the errors obtained with the three methods implemented on the three sets of trajectories; for better readability, a bar-plot representation of these same data is also shown in Figs. 6–8.

TABLE I
NORMALIZED ODOMETRIC ERRORS FOR THREE IDENTIFICATION METHODS IMPLEMENTED ON THE KHEPERA II

exp		position error			orientation error		
		A	B	C	A	B	C
set1	max	2.1	**2.0**	3.9	3.4	**3.1**	4.6
	mean	0.9	**0.6**	1.7	0.3	**0.07**	0.8
	std	0.9	**0.8**	1.3	**1.9**	**1.9**	2.2
set2	max	1.9	2.1	**1.3**	1.8	2.0	**0.8**
	mean	1.0	1.4	**0.09**	0.5	0.4	**0.06**
	std	**0.5**	**0.5**	**0.5**	0.8	1.1	**0.3**
set3	max	6.7	6.7	**3.9**	5.8	5.9	**3.8**
	mean	2.6	2.9	**1.1**	2.2	2.0	**1.1**
	std	1.8	1.8	**1.5**	2.2	2.4	**1.7**

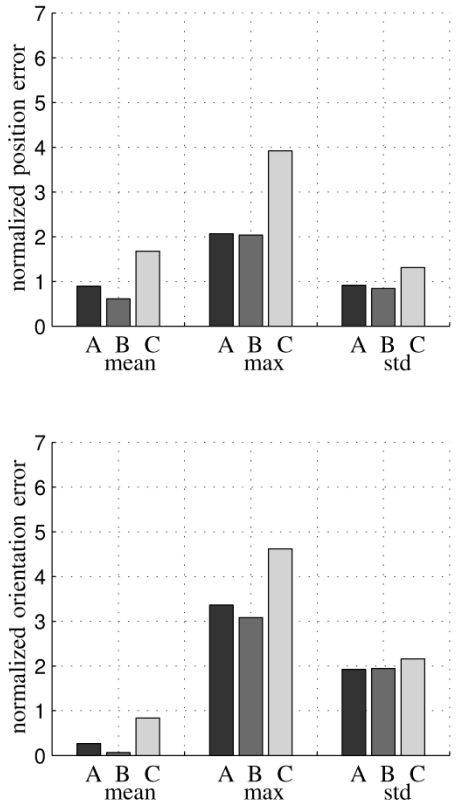

Fig. 6. Normalized odometric errors obtained on **set1** with the three calibration methods implemented on the Khepera II. Notice that **set1** includes the same data of the test trajectories of Method B).

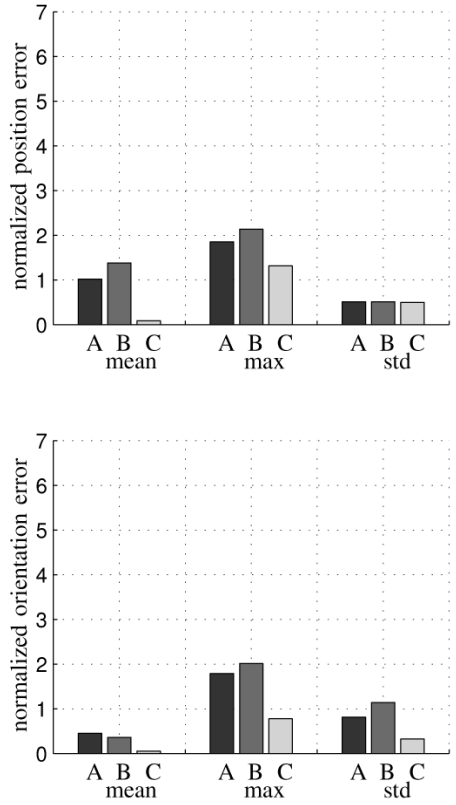

Fig. 7. Normalized odometric errors obtained on **set2** with the three calibration methods implemented on the Khepera II. Notice that **set2** includes the same data of the test trajectories of Method C).

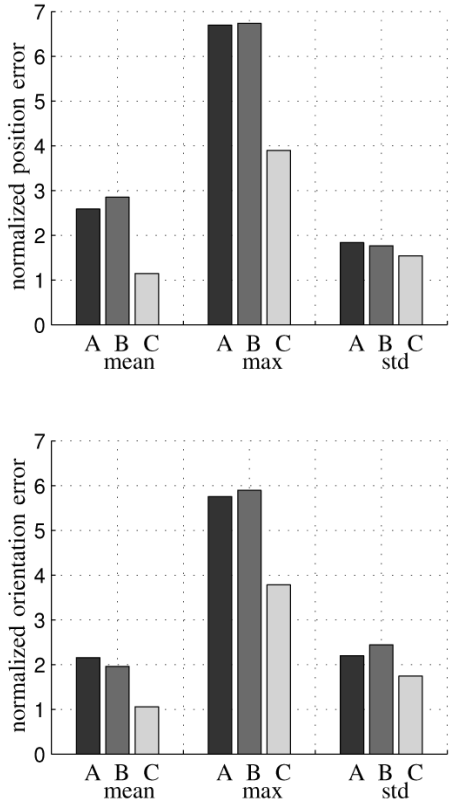

Fig. 8. Normalized odometric errors obtained on **set3** with the three calibration methods implemented on the Khepera II.

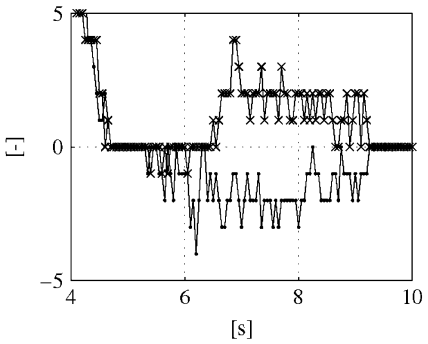

Fig. 9. Angular velocity of the wheels along a 4-s turn of 90°. A high level of quantization can be observed.

From the reported data, overall the three methods worked in these experiments with similar performance. Since the three calibration methods considered range from a pure parameter-based technique with no motion-based external measures (Method A), to a technique fully based on test-motion data (Method C), through a mixed technique (Method B), this would suggest that on the scale of these experiments, accuracy of the external measurements does not outperform accuracy yield by model-based calculations. On the other hand, the Khepera II has a very clean mechanical design and realization, while our vision-based measurement system has limited per-pixel precision.

One other thing to be remarked is the presence of major unmodeled nonlinear effects. In fact, the Khepera II shows a significant quantization error affecting the angular velocity of the wheels; this is indeed expressed as an integer in the range ± 127, where one unit corresponds to a vehicle velocity of 8 mm/s in case of a pure translation, or of 9 deg/s in case of a pure rotation. To illustrate the relevance of this effect, Fig. 9 shows the time history of the angular velocity of the two wheels while the robot executes a 90° turn in 4 s.

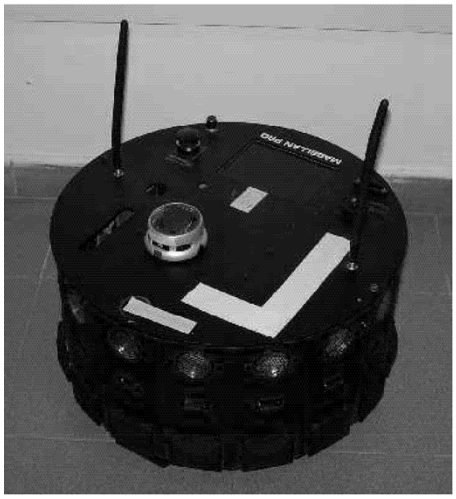

Fig. 10. Magellan PRO mobile robot and the L-shaped model used to estimate its position and orientation. To illustrate the relative dimensions, the robot Khepera II is placed on the Magellan PRO.

To check on this matter, Methods B) and C) have been applied in a simulation case study in the absence of nonsystematic errors and nonmodeled dynamics; a white Gaussian noise has been added to the measurements. The obtained results are not reported here for brevity, but can be summarized as follows. Starting from a perfect knowledge of the wheel diameter, Method B) gave excellent performance. With an equal number of experiments, Method C) seems to be more sensitive than Method B) to the measurement noise; however, the sensitivity is lowered by increasing the number of experiments. On the other hand, Method B) is sensitive to errors in the measurement of the wheel diameter.

D. Experiments With Magellan PRO

The proposed odometry-calibration technique has been validated also in experiments run with the Magellan PRO mobile robot, shown in Fig. 10, manufactured by Real World Interface [1].

The sampling period used is 25 ms, which corresponds to the highest rate at which the Magellan PRO operating system makes the sensory data available to the user. Same as for the Khepera II, to avoid slippage of the wheels, all the trajectories have blended polynomial time laws that guarantee continuity of the acceleration variables all over the motion. Notice that, unless differently stated, in this subsection, the lengths are reported in meters and the angles in radians.

1) Tailoring the Proposed Algorithm to the Available Hardware: The Magellan PRO mobile robot is not a prototype, and part of the control code is binary. In particular, the measurements of ω_R, ω_L are not available to the user, while the code provides the nominal value of the linear velocity v_n and angular velocity ω_n of the vehicle; these are computed through the mapping

$$\begin{bmatrix} v_n \\ \omega_n \end{bmatrix} = \begin{bmatrix} \hat{r}_R/2 & \hat{r}_L/2 \\ \hat{r}_R/\hat{b} & -\hat{r}_L/\hat{b} \end{bmatrix} \begin{bmatrix} \omega_R \\ \omega_L \end{bmatrix} = C_n \begin{bmatrix} \omega_R \\ \omega_L \end{bmatrix} \tag{22}$$

where the values of $\hat{r}_R$, $\hat{r}_L$, and $\hat{b}$ estimated and used by the vehicle developers are unknown to the end user.

For that, the mapping to be identified in our experiments is obtained by combining (1) with the inverse of (22), leading to

$$\begin{bmatrix} v \\ \omega \end{bmatrix} = C C_n^{-1} \begin{bmatrix} v_n \\ \omega_n \end{bmatrix} = \overline{C} \begin{bmatrix} v_n \\ \omega_n \end{bmatrix} \tag{23}$$

where the matrix $\bar{C}$ is given by

$$\bar{C} = \begin{bmatrix} \dfrac{r_R}{2\hat{r}_R} + \dfrac{r_L}{2\hat{r}_L} & \dfrac{\hat{b}r_R}{4\hat{r}_R} - \dfrac{\hat{b}r_L}{4\hat{r}_L} \\ \dfrac{r_R}{b\hat{r}_R} - \dfrac{r_L}{b\hat{r}_L} & \dfrac{\hat{b}r_R}{2b\hat{r}_R} + \dfrac{\hat{b}r_L}{2b\hat{r}_L} \end{bmatrix}. \tag{24}$$

The overall reconstruction scheme is summarized in Fig. 11, where sampling of the measured data is also evidenced.

In the case of perfect knowledge of the odometric parameters, i.e., $\hat{r}_R = r_R$, $\hat{r}_L = r_L$, and $\hat{b} = b$, the matrix $\bar{C}$ is the identity matrix. In particular, nonnull off-diagonal terms are responsible for cross-coupling, e.g., a turn is felt when a straight-line nominal motion is executed.

Strictly speaking, the algorithm described in Section III cannot be applied to the Magellan PRO, since measurement of ω_R and ω_L is not available. However, the proposed technique can be easily adapted to our system through proper redefinition of the regressors $\mathbf{\Phi}_\theta$ and $\mathbf{\Phi}_{xy}$. In fact, by observing that in our case, the couple $\{v_n, \omega_n\}$ plays the role of the couple $\{\omega_R, \omega_L\}$, a symbolic substitution in (7) and (13) leads to the expression

$$\mathbf{\Phi}_\theta = T \begin{bmatrix} \displaystyle\sum_{i=0}^{N-1} v_{n,i} & \displaystyle\sum_{i=0}^{N-1} \omega_{n,i} \end{bmatrix} \tag{25}$$

for the orientation regressor, while the position regressor becomes

$$\mathbf{\Phi}_{xy} = T \begin{bmatrix} \sum_{i=0}^{N-1} v_{n,i} \cos(\theta_i + T\omega_i/2) & \sum_{i=0}^{N-1} \omega_{n,i} \cos(\theta_i + T\omega_i/2) \\ \sum_{i=0}^{N-1} v_{n,i} \sin(\theta_i + T\omega_i/2) & \sum_{i=0}^{N-1} \omega_{n,i} \sin(\theta_i + T\omega_i/2) \end{bmatrix}. \tag{26}$$

Obviously, the same formulas as in (10) and (14) give, in our case, the LS estimate of the unknown odometric parameters $\bar{c}_{i,j}$, with $i, j = 1, 2$.

2) Experimental Results: In the case of the Magellan PRO, the calibration has been performed by resorting to two different methods:

C) the technique proposed in this paper;

D) the odometry of the manufacturer.

Application of the Method C) requires the execution of suitable test motions. To achieve a large norm of the data vector while keeping a small condition number of the regressors, we have chosen in this case 10 L-shaped open paths of 0.7-m side. The time law is a blend of fifth-order polynomials. To avoid compensation of the errors, each path is described both in the CW and in the CCW direction, leading to a set of 20 trajectories (briefly **set4** in the following). The data collected by the test trajectories result in the regressors' condition numbers

$$\begin{aligned} \mathrm{cond}(\bar{\mathbf{\Phi}}_\theta) &= 2.27 \\ \mathrm{cond}(\bar{\mathbf{\Phi}}_{xy}) &= 2.00 \end{aligned}$$

in the data vectors' norm

$$\left\| \begin{bmatrix} \theta_{N,1} - \theta_{0,1} \\ \vdots \\ \theta_{N,20} - \theta_{0,20} \end{bmatrix} \right\| = 14.25$$

$$\left\| \begin{bmatrix} x_{N,1} - x_{0,1} \\ y_{N,1} - y_{0,1} \\ \vdots \\ x_{N,20} - x_{0,20} \\ y_{N,20} - y_{0,20} \end{bmatrix} \right\| = 4.34$$

and in the smallest singular values

$$\begin{aligned} \lambda_{\min}(\bar{\mathbf{\Phi}}_\theta) &= 6.34 \\ \lambda_{\min}(\bar{\mathbf{\Phi}}_{xy}) &= 4.52. \end{aligned}$$

In view of the very small condition number, these values guarantee that numerical problems are avoided [cfr. (16) and (18)]. The $\bar{C}$ matrix obtained by Method C) is

$$\bar{C}_C = \begin{bmatrix} 0.95959 & -0.00074 \\ 0.01029 & 0.98764 \end{bmatrix}.$$

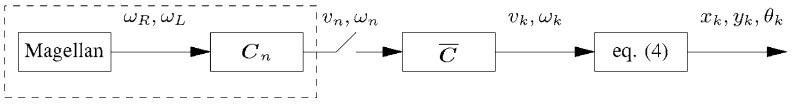

Fig. 11. Kinematic transformation between the measured variables and the body-fixed vehicle velocities for the Magellan PRO. In the dashed box are the unaccessible variables.

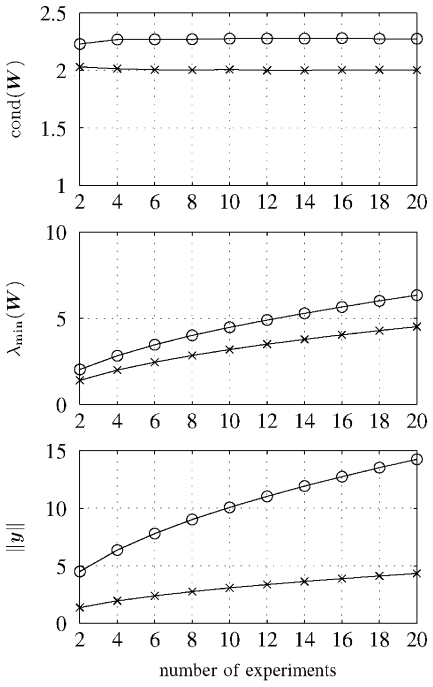

Fig. 12. Condition number of the regressors (top), minimum singular value of the regressors (center), and norm of the measurement data vector (bottom) versus the number of experiments for the orientation LS problem ($\circ$) and the position LS problem ($\times$).

TABLE II
NORMALIZED ODOMETRIC ERRORS FOR TWO IDENTIFICATION METHODS IMPLEMENTED ON MAGELLAN PRO

exp		position error C	position error D	orientation error C	orientation error D
set4	max	**3.6**	3.8	**2.1**	3.1
	mean	**0.2**	1.6	**0.008**	0.3
	std	1.4	**1.2**	**0.9**	1.6
set5	max	**1.7**	3.8	**0.4**	2.3
	mean	**0.3**	2.3	**0.02**	0.6
	std	**0.8**	1.5	**0.3**	1.9

To verify that increasing the number of experiments actually improves accuracy of the calibration procedure, it is interesting to monitor the condition number and the minimum singular value of the regressors, and the norm of the measurement vector as a function of the number of times the trajectory is executed. These are reported in Fig. 12, where only sets of three motions composed of one CW and one CCW are considered significant. It can be recognized that while just one set of experiments allows minimizing the condition number of both regressors, the norm of the measurement vector (that grows with the square root of the number of experiments) is still significantly raised after 20 runs.

As remarked in Section V-D.1, perfect knowledge of the odometric parameters leads to an identity $\bar{C}$ matrix; therefore, under Method D), it is

$$\bar{C}_D = \begin{bmatrix} 1 & 0 \\ 0 & 1 \end{bmatrix}.$$

After the two calibrations, other trajectories have been run to validate the two obtained odometries and to evaluate the experimental results. Overall, the following sets of trajectories have been considered:

- **set4** 20 trajectories, 10 CW and 10 CCW, over a L-shaped path of 0.7-m side;
- **set5** four trajectories, two CW and two CCW, over a square path of 0.7-m side.

Notice that the **set4** trajectories include also those used for calibration Method C), while the **set5** trajectories include pure validation data. Table II reports the errors obtained with the two methods implemented on the two sets of trajectories; for better readability, a bar-plot representation of these same data is also shown in Figs. 13 and 14.

The reported data show a good performance of the proposed method, with particular reference to the mean normalized error. On the other hand, in comparison with the Khepera II, while the larger geometry of the Magellan PRO allows more accurate vision-based measurements, it results in a less clean mechanical realization; this would explain the benefit experienced in this case by using external measurements over pure model-based calculations.

As a curiosity, it can be noticed that in view of (23) with the nominal $\bar{C}$ being the identity matrix, the calibrated odometry allows easily reading the error of the nominal odometry. In fact, the singular values of the matrix $\bar{C}_D$ give an estimate of the odometric error: greater-than-one (smaller-than-one) singular values correspond to traveled paths longer (shorter) than the planned length. For close-to-identity matrices, such as the one obtained in our case, the diagonal terms well approximate the singular values of $\bar{C}_D$: being $\bar{c}_{1,1}$ and $\bar{c}_{2,2}$ smaller than unity, our vehicle travels paths of slightly smaller length (angle) than the nominal ones.

3) Identification of the Off-Diagonal Elements of $\bar{C}$: It can be observed that despite the good numerical conditioning of the identification problem, the unknowns are badly scaled, since a difference of two orders of magnitude exists between the diagonal and the off-diagonal elements of $\bar{C}$.

According to (19), a better numerical balance might be obtained considering a weighted regressor; however, by considering the data collected and the first estimation of the unknowns, the two condition numbers for the orientation and the position regressors would result in a value of 220 and 650, respectively. In words, it means that the off-diagonal elements are badly identified because of numerical reasons; this calls for the design of specific trajectories that better fit the way those elements affect the odometry of the mobile robot.

The element $\bar{c}_{1,2}$ quantifies the coupling effect existing between the commanded nominal angular velocity of the vehicle and its actual translational velocity. In the ideal case of perfect odometry it would be zero, whereas in our case, it is of the order of 10^{-3}. Let us compute the x-component of the vehicle position as

$$x = \int v \cos(\theta)\, \mathrm{d}t = \int (\bar{c}_{1,1}\, v_n + \bar{c}_{1,2}\, \omega_n) \cos(\theta)\, \mathrm{d}t. \qquad (27)$$

In order to emphasize the effect of the commanded angular velocity on the vehicle translation, and thus magnify the contribution of the element $\bar{c}_{1,2}$ to the robot odometry, a pure constant rotation (i.e., $v_n = 0$ with $\omega_n = \hat{\omega}_n$) can be commanded, leading to

$$x = \int \bar{c}_{1,2}\, \hat{\omega}_n \cos(\theta)\, \mathrm{d}t. \qquad (28)$$

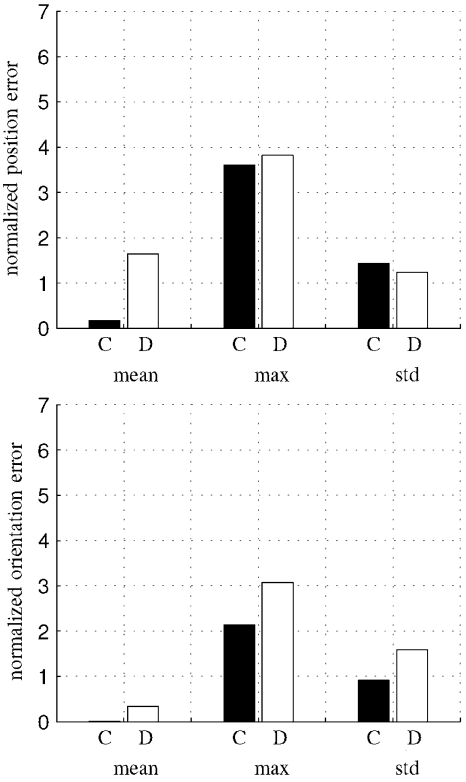

Fig. 13. Normalized odometric errors obtained on **set4** with the two calibration methods implemented on the Magellan PRO. Notice that **set4** includes the same data of the test trajectories of Method C).

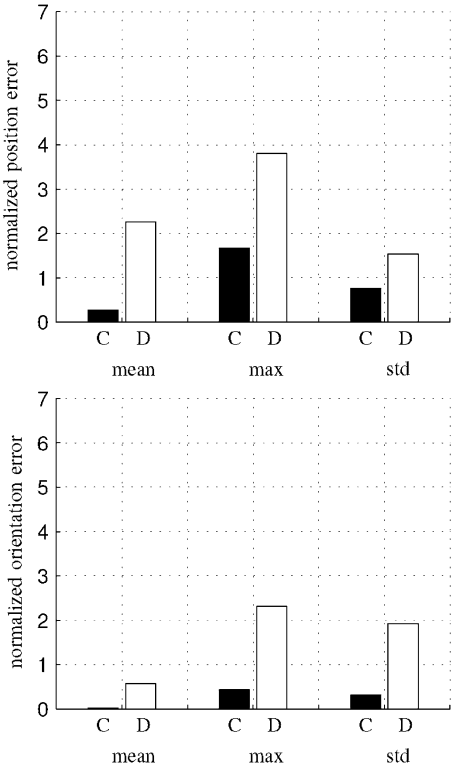

Fig. 14. Normalized odometric errors obtained on **set5** with the two calibration methods implemented on the Magellan PRO.

With a constant angular velocity $\hat{\omega}_n$, it is

$$\theta(t) = \bar{c}_{2,2}\,\hat{\omega}_n\,t$$

thus, (28) over a duration t_f yields

$$x = \frac{\bar{c}_{1,2}}{\bar{c}_{2,2}}\sin(\bar{c}_{2,2}\,\hat{\omega}_n\,t_f). \tag{29}$$

The same argument applied to the y-component of the vehicle position leads to a similar result

$$y = \frac{\bar{c}_{1,2}}{\bar{c}_{2,2}}\cos(\bar{c}_{2,2}\,\hat{\omega}_n\,t_f). \tag{30}$$

It is easy to recognize that along either component, the coupling effect between the commanded nominal angular velocity of the vehicle and its actual translational velocity is of the order of the ratio $\bar{c}_{1,2}/\bar{c}_{2,2}$. In our case, this ratio is on the order of millimeters, $\bar{c}_{2,2}$ being close to unity. Since for our experimental setup nonsystematic errors (due, e.g., to friction and backlash) are of the same order of magnitude than the systematic errors (29), (30), it is not possible to significantly improve the estimate of $\bar{c}_{1,2}$ over the obtained result, even with specifically designed test motions.

On the other hand, the element $\bar{c}_{2,1}$ quantifies the coupling effect existing between the commanded nominal translational velocity of the vehicle and its actual angular velocity. In the ideal case of perfect odometry, it would be zero, whereas in our case, it is on the order of 10^{-2}. Different from the other off-diagonal element of $\bar{\boldsymbol{C}}$, the element $\bar{c}_{2,1}$ can be identified in our case. In fact, repeating the same reasoning as above and selecting a pure constant translation (i.e., $v_n = \hat{v}_n$ with $\omega_n = 0$) yields

$$\theta(t_f) = \bar{c}_{2,1}\,\hat{v}_n\,t_f \tag{31}$$

meaning that a suitably long straight path (i.e., one with a large product $\hat{v}_n t_f$ that results in a suitably large rotation $\theta(t_f)$) allows reliably computing $\bar{c}_{2,1}$. From a practical point of view, however, the longer the path, the higher the possibility of experiencing the effects of nonsystematic errors; this suggests avoiding longer paths than necessary.

VI. Summary of Steps Required to Implement the Proposed Method

1) Setting up a measurement system such as the vision-based system described in this paper or a sonar-based system, described in [8].
2) Planning a motion for the vehicle following the guidelines given in Section IV.
3) Execute the tests and collect, for each trajectory, the vehicle configuration before and after the movement and the right and left wheels angular velocities ω_R and ω_L during the motion.
4) In (9), compute the left-hand side vector and its norm, compute the matrix $\bar{\boldsymbol{\Phi}}_\theta$ with the corresponding condition number and minimum singular value. Check appropriateness of the numerical values, in case, add or modify the test trajectories.
5) Compute $\hat{c}_{2,1}$ and $\hat{c}_{2,2}$ using (10).
6) For the collected data, update the estimation of θ_k by using (4) with the correct estimation of ω_k achieved by using the second row of matrix $\boldsymbol{C}$ in (2).
7) Compute the stacked vector in (12) and its norm, compute the stacked matrix $\bar{\boldsymbol{\Phi}}_{xy}$ in (13) with the corresponding condition number and minimum singular value. Check appropriateness of the numerical values, in case, add or modify the motion data. Notice that the corrected values for θ_k and ω_k need to be used.
8) Compute $\hat{c}_{1,1}$ and $\hat{c}_{1,2}$ using (14).
9) Validate the identification by computing the odometric errors using (4) and (2).

VII. Conclusion

In this paper, a new method for odometry calibration of differential-drive mobile robots has been presented. The proposed method realizes the estimate of a suitable set of odometric parameters for which a linear identification problem is posed. Because of the linear nature of the problem, the developed solution is derived in the framework of the LS approach; therefore, an advantage of our technique lies in the possibility of evaluating the numerical conditioning of the collected data. Different from previous methods, the proposed approach can be implemented on a variety of trajectories and not on a single predefined path, thus allowing more ease for practical implementation. Extensive experimental case studies have been performed with the Khepera II and Magellan PRO mobile robots, and the obtained results confirm the effectiveness of the proposed calibration method.

Acknowledgment

The authors thank R. Choubisa of the Indian Institute of Technology, Kanpur, India, for his help in performing the vision-based experiments.

References

[1] Real World Interface [Online]. Available: http://www.irobot.com/rwi/
[2] K-Team [Online]. Available: http://www.k-team.com/
[3] Matrox Electronic Systems Ltd., "Matrox Imaging Library User Guide," Matrox Electronic Systems Ltd., Dorval, QC, Canada, 2001.
[4] G. Antonelli, S. Chiaverini, and G. Fusco, "Exciting trajectories for mobile robot odometry calibration," in *Preprints 7th IFAC Symp. Robot Control*, Wroclaw, Poland, Sep. 2003, pp. 429–434.
[5] ——, "An odometry calibration method for mobile robots based on the least-squares technique," in *Proc. Amer. Control Conf.*, Denver, CO, Jun. 2003, pp. 3429–3434.
[6] P. Bonnifait, P. Bouron, P. Croubillé, and D. Meizel, "Data fusion of four ABS sensors and GPS for an enhanced localization of car-like vehicles," in *Proc. IEEE Int. Conf. Robot. Autom.*, Seoul, Korea, May 2001, pp. 1597–1602.
[7] J. Borenstein, "Experimental results from internal odometry error correction with the OmniMate mobile robot," *IEEE Trans. Robot. Autom.*, vol. 14, no. 6, pp. 963–969, Dec. 1998.
[8] J. Borenstein and L. Feng, "Measurement and correction of systematic odometry errors in mobile robots," *IEEE Trans. Robot. Autom.*, vol. 12, no. 6, pp. 869–-880, Dec. 1996.
[9] K. S. Chong and L. Kleeman, "Accurate odometry and error modeling for a mobile robot," in *Proc. IEEE Int. Conf. Robot. Autom.*, Albuquerque, NM, May 1997, pp. 2783–2788.
[10] I. J. Cox, "Blanche—An experiment in guidance and navigation of an autonomous robot vehicle," *IEEE Trans. Robot. Autom.*, vol. 7, no. 2, pp. 193–204, Apr. 1991.
[11] N. Doh, H. Choset, and W. K. Chung, "Accurate relative localization using odometry," in *Proc. IEEE Int. Conf. Robot. Autom.*, Taipei, Taiwan, 2003, pp. 1606–1612.
[12] P. Goel, S. I. Roumeliotis, and G. S. Sukhatme, "Robust localization using relative and absolute position estimates," in *Proc. IEEE/RSJ Int. Conf. Intell. Robots Syst.*, Kyongju, Korea, Oct. 1999, pp. 1134–1140.
[13] G. H. Golub and C. F. Van Loan, *Matrix Computations*, 3rd ed. Baltimore, MD: Johns Hopkins Univ. Press, 1996.
[14] S. Hutchinson, G. D. Hager, and P. I. Corke, "A tutorial on visual servo control," *IEEE Trans. Robot. Autom.*, vol. 12, no. 5, pp. 551–570, Oct. 1996.
[15] A. Kelly, "General solution for linearized systematic error propagation in vehicle odometry," in *Proc. IEEE/RSJ Int. Conf. Intell. Robots Syst.*, Maui, HI, Nov. 2001, pp. 1938–1945.
[16] ——, "General solution for linearized stochastic error propagation in vehicle odometry," in *Preprints 15th IFAC World Congr.*, Barcelona, Spain, Jul. 2002.
[17] K. Komoriya and E. Oyama, "Position estimation of a mobile robot using optical fiber gyroscope (OFG)," in *Proc. IEEE/RSJ Int. Conf. Intell. Robots Syst.*, Munich, Germany, Sep. 1994, pp. 143–149.
[18] L. Ljung, *System Identification: Theory for the User*. Upper Saddle River, NJ: Prentice-Hall, 1999.
[19] A. Martinelli, "The accuracy on the parameter estimation of an odometry system of a mobile robot," in *Proc. IEEE Int. Conf. Robot. Autom.*, Washington, DC, May 2002, pp. 1378–1383.
[20] ——, "The odometry error of a mobile robot with a synchronous drive system," *IEEE Trans. Robot. Autom.*, vol. 18, no. 3, pp. 399–405, Jun. 2002.
[21] C. Presse and M. Gautier, "New criteria of exciting trajectories for robot identification," in *Proc. IEEE Int. Conf. Robot. Autom.*, Atlanta, GA, 1993, pp. 907–912.
[22] N. Roy and S. Thrun, "Online self-calibration for mobile robots," in *Proc. IEEE Int. Conf. Robot. Autom.*, Detroit, MI, May 1999, pp. 2292–2297.
[23] H. J. von der Hardt, R. Husson, and D. Wolf, "An automatic calibration method for a multisensor system: Application to a mobile robot localization system," in *Proc. IEEE Int. Conf. Robot. Autom.*, Leuven, Belgium, 1998, pp. 3141–3146.
[24] C. M. Wang, "Location estimation and uncertainty analysis for mobile robots," in *Proc. IEEE Int. Conf. Robot. Autom.*, Philadelphia, PA, 1988, pp. 1230–1235.

Multiview Camera-Calibration Framework for Nonparametric Distortions Removal

Christophe Y. Vincent and Tardi Tjahjadi

***Abstract*—This paper proposes a technique that uses a planar calibration object and projective constraints to calibrate parametric and nonparametric distortions. An iterative surface fitting is first used to constrain a B-spline distortion model by fusing the corrective distortion maps obtained from multiple views. The model is then refined within the whole camera-calibration process.**

***Index Terms*—Camera calibration, geometric modeling, image distortion, splines, surface fitting.**

I. Introduction

Camera calibration, a process of determining camera intrinsic parameters has been extensively studied [1]. Three families of calibration methods can be identified. The first family uses a known calibration object (e.g., [2]) comprising three-dimensional (3-D) features or 2-D features with an unknown displacement of a planar calibration object [3] to simultaneously estimate different sets of camera extrinsic parameters (multiview approach). The second family uses geometric invariance of image features (e.g., [4]), rather than their locations. The third family, commonly known as self-calibration methods (e.g., [5]), exploit natural features of a structured environment rather than a calibration object for fixed camera parameters.

The precision in the camera calibration depends mainly on two factors. The first is the accuracy of the feature detection, thus, the type of features, too. The second is the type of camera model chosen according to the type of camera lenses used, as different lenses induce different amount and types of distortions. We refer to these parametric deviations from the pinhole model as parametric distortions. Numerous

Manuscript received December 8, 2004; revised April 1, 2005. This work was supported by the U.K. Department of Trade and Industry as part of the Foresight Vehicle Link Programme. This paper was recommended for publication by Associate Editor H. Zhuang and Editor F. Park upon evaluation of the reviewers' comments.

The authors are with the School of Engineering, University of Warwick, Coventry CV4 7AL, U.K. (e-mail: tt@eng.warwick.ac.uk).

Digital Object Identifier 10.1109/TRO.2005.851383